Final Report for AOARD Grant FA2386-11-1-4101

"**Effect of grain scale properties on bulk deformation of granular deposit due to high speed projectile impact**"

April 8, 2013

Name of Principal Investigators: Takashi Matsushima

- e-mail address : tmatsu@kz.tsukuba.ac.jp
- Institution : University of Tsukuba
- Mailing Address : 1-1-1, Tennodai, Tsukuba, Ibaraki, 305-8573, Japan
- Phone : +81-29-853-5269
- Fax : +81-29-853-5207

Period of Performance: Sept. 1, 2011 – March 31, 2013

Abstract:

In order to understand the mechanical behavior of granular deposit subjected to high-speed projectile impact, we perform both physical experiments and grain-scale numerical simulations. In the high-speed impact experiment, we adopted a new technology to observe the deceleration of projectile after penetrating into sand layer. The observed results together with simple one-dimensional model with Rankine-Hugoniot equations suggests the importance of grain-scale mechanics such as grain crushing to evaluate the evolution of material parameters.

Grain-scale observation of the specimen after the experiment by micro x-ray CT revealed that the grain crushing is a key phenomenon for evaluating projectile motion. Then a series of numerical simulation using Discrete Element Method were performed and the compression behavior of granular materials was analyzed in terms of grain crushing. The results suggest the transition of three material phases; (1) elastic regime as a granular matter, (2) plastic regime due to grain crushing, and (3) Hugoniot solid regime, and they are the important ingredients for modeling the equation of state of granular materials subjected to high speed compression.

Based on the above-mentioned observations, we constructed the EOS which covers wide range of deformation rate; from quasi-static deformation to high-speed impact, because the projectile deceleration process is affected not only by the initial high-speed regime but also the subsequent slow deformation regime. The proposed EOS was validated both with the existing impact experiment and with the quasi-static 1D compression test. Moreover, we also found that the material parameters for granular materials can be obtained from those for the host rock.

Finally, we demonstrated the applicability of the proposed EOS into high-speed projectile impact experiment. It turned out that the projectile deceleration behavior observed in the experiment is a consequence of the complicated compression behavior of sand deposit.

1. Introduction:

High speed impact problem has been of great concern in various science communities. In particular, the high speed projectile impact to granular deposit (e.g., sand deposit) has been extensively studied in many research fields. Planetary science, for example, requires the mechanical information on meteoroid impact to planets and asteroids in order to understand the formation and evolution process of their surface morphology and material [1, 2]. Material science has dealt with the high impact behavior for new material productions and processes [3]. Civil engineering researchers have been studied the stability of soil ground and earth structures against the projectile impact or explosion [4]. In spite of such tremendous history, we still do not fully understand the whole phenomena, primarily because the granular material itself is a material full of complexity [5,6], and also because

Report Documentation Page

Form Approved
OMB No. 0704-0188

1. REPORT DATE	2. REPORT TYPE	3. DATES COVERED
15 APR 2013	**Final**	**14-09-2011 to 13-02-2012**

4. TITLE AND SUBTITLE
Effect of Grain Scale Properties on Bulk Deformation of Granular Deposits Due to High Speed Projectile Impact

5a. CONTRACT NUMBER
FA23861114101

5b. GRANT NUMBER

5c. PROGRAM ELEMENT NUMBER

6. AUTHOR(S)
Matsushima Takashi

5d. PROJECT NUMBER

5e. TASK NUMBER

5f. WORK UNIT NUMBER

7. PERFORMING ORGANIZATION NAME(S) AND ADDRESS(ES)
UNIVERSITY OF TSUKUBA,1-1-1, TENNODAI,TSUKUBA 305-0006,JAPAN,NA,NA

8. PERFORMING ORGANIZATION REPORT NUMBER
N/A

9. SPONSORING/MONITORING AGENCY NAME(S) AND ADDRESS(ES)
AOARD, UNIT 45002, APO, AP, 96338-5002

10. SPONSOR/MONITOR'S ACRONYM(S)
AOARD

11. SPONSOR/MONITOR'S REPORT NUMBER(S)
AOARD-114101

12. DISTRIBUTION/AVAILABILITY STATEMENT
Approved for public release; distribution unlimited

13. SUPPLEMENTARY NOTES

14. ABSTRACT

In order to understand the mechanical behavior of granular deposit subjected to high-speed projectile impact, we perform both physical experiments and grain-scale numerical simulations. In the high-speed impact experiment, we adopted a new technology to observe the deceleration of projectile after penetrating into sand layer. The observed results together with simple one-dimensional model with Rankine-Hugoniot equations suggests the importance of grain-scale mechanics such as grain crushing to evaluate the evolution of material parameters. Grain-scale observation of the specimen after the experiment by micro x-ray CT revealed that the grain crushing is a key phenomenon for evaluating projectile motion. Then a series of numerical simulation using Discrete Element Method were performed and the compression behavior of granular materials was analyzed in terms of grain crushing. The results suggest the transition of three material phases; (1) elastic regime as a granular matter, (2) plastic regime due to grain crushing, and (3) Hugoniot solid regime, and they are the important ingredients for modeling the equation of state of granular materials subjected to high speed compression. Based on the above-mentioned observations, we constructed the EOS which covers wide range of deformation rate; from quasi-static deformation to high-speed impact, because the projectile deceleration process is affected not only by the initial high-speed regime but also the subsequent slow deformation regime. The proposed EOS was validated both with the existing impact experiment and with the quasi-static 1D compression test. Moreover, we also found that the material parameters for granular materials can be obtained from those for the host rock. Finally, we demonstrated the applicability of the proposed EOS into high-speed projectile impact experiment. It turned out that the projectile deceleration behavior observed in the experiment is a consequence of the complicated compression behavior of sand deposit.

15. SUBJECT TERMS

Solid Mechanics, penetration mechanics, Shock Waves

16. SECURITY CLASSIFICATION OF:			17. LIMITATION OF ABSTRACT	18. NUMBER OF PAGES	19a. NAME OF RESPONSIBLE PERSON
a. REPORT	b. ABSTRACT	c. THIS PAGE			
unclassified	**unclassified**	**unclassified**	**Same as Report (SAR)**	**24**	

some additional physics such as shock wave transmission [7] and material melting [8] are included in the impact phenomena.

According to Reference [2], the behavior of granular deposit due to high speed projectile impact is divided into three stages for better comprehension: (a) contact and compression stage, (b) excavation stage, and (c) modification stage. In stage (a), material compressibility plays an important role, while incompressible fluid model [9] is often assumed in stage (b). Stage (c) is related to the more solid-like nature of granular materials. These stages are characterized by the deformation velocity range of the material. In order to simulate the whole behavior it is inevitable not only to observe the phenomenon of each stage in details, but also to develop the unified description being valid throughout the wide range of deformation speed; from quasi-static deformation to high-speed deformation over 1km/sec.

Quasi-static deformation has been studied mainly in geotechnical engineering field, while high-rate shear has been studied in physics and powder engineering. In addition, high-speed impact problem associated with grain crushing and melting due to shock wave has been studied in astrophysics and military engineering. These fields have their own disciplines and there is no unified perspective so far. Therefore, it is quite important to make an interdisciplinary discussion over the societies [10].

This research project aims at better understanding and modeling the whole process of projectile impact to granular deposit using experimental and numerical tools. First, we present some results of impact experiments in which a new technology is adopted to measure the deceleration of projectile penetrating into sand layer. The observed velocity-displacement relation is compared with a conceptual one-dimensional model at first, and then is quantitatively evaluated with Rankine-Hugoniot equations. Through this analysis, it is pointed that the material parameters for the equation of state of granular materials should be examined in more details. In particular, considerable grain crushing is observed in the impact experiment, which has to be taken into account. For this purpose, a series of numerical simulation using Discrete Element Method have been performed, and the relation between the compressive stress and strain is examined in terms of grain crushing behavior. The results suggest the transition of three material phases; (1) elastic regime as a granular matter, (2) plastic regime due to grain crushing, and (3) Hugoniot solid regime.

Finally we summarize this annual report with some future research perspectives.

2. High-speed impact experiment:

Large scale vertical powder gun is used to perform impact experiments in which a cylindrical projectile (15mm in diameter and 26mm in length) vertically hit to a sand deposit in a PMMA

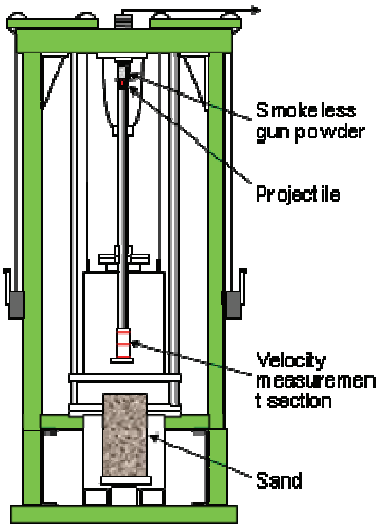

Fig. 1 Vertical powder gun.

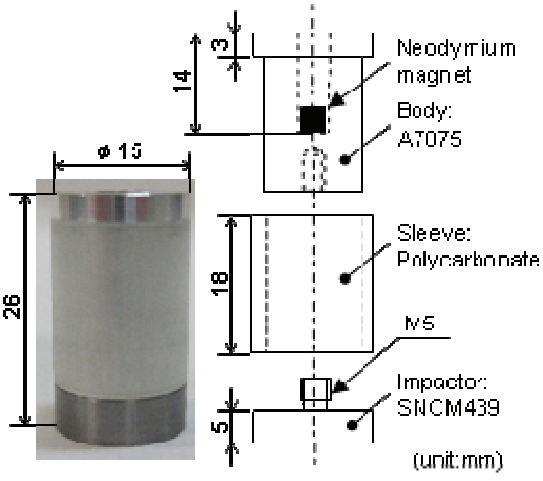

Fig. 2 Projectile embedding magnet

container (100mm in inner diameter and 300mm in inner depth) with a speed of about 500 m/sec (Figs.1 and 2). Sand material is the Florida coastal sand largely consisting of quartz whose grain size ranges from 0.1mm to 1mm (Figs 3 and 4).
A high resolution high speed camera is used to observe the surface deformation of the granular deposit (Figs.5 and 6). The earth pressure change due to projectile penetration is measured by high response pressure gauges. Small thermocouples are also used to heat transfer in the granular deposit. Moreover, an originally developed devices using electromagnetic induction (Fig.7) are applied to clarify the location of projectile after penetrating into the granular deposit. It allows us the multi-point measurement of the

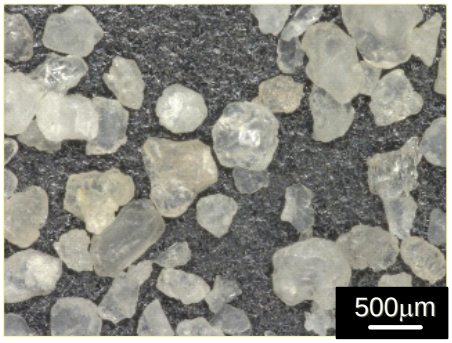

Fig. 3 Micrograph of sand (Florida coastal sand).

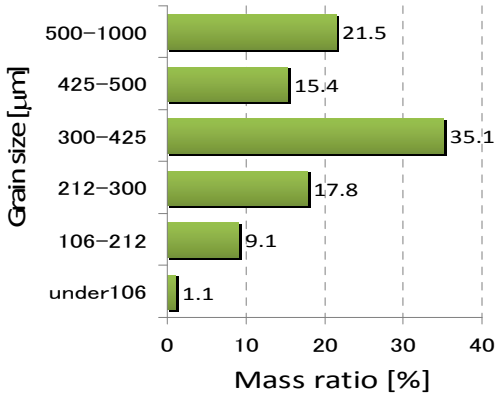

Fig. 4 Grain size distribution

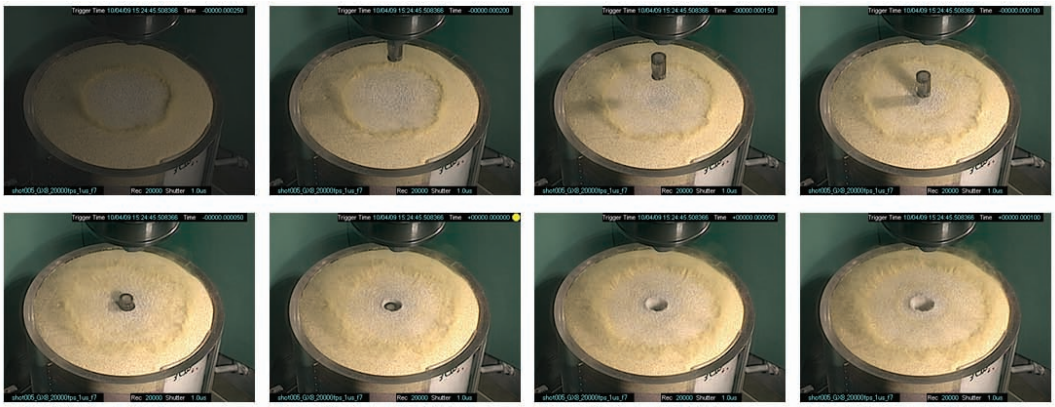

Fig.5 High-speed visualization of behavior of projectile during penetration. (Frame rate; 20,000 fps, exposure time; 1ms, impact velocity; 495 m/s.)

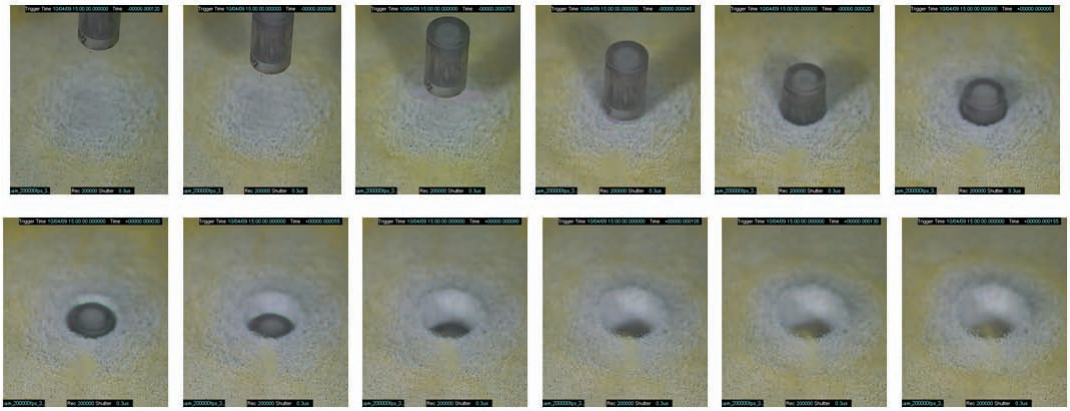

Fig. 6 High-speed visualization of detailed behavior of projectile during penetration. (Frame rate; 200,000 fps (every 5 frames), exposure time; 300 ns, impact velocity; 495 m/s.)

location of a moving magnet in opaque media like sands. We just embed a magnet in a projectile which results in a minimal disturbance of sand and projectile. The setup is relatively inexpensive and easy to handle. We have already confirmed that it has sufficient measurement accuracy.

Fig.8 shows an example of the deceleration of the projectile during the penetration into the sand deposit. In order to understand the feature of this time history of the projectile velocity v, we consider the following simple equation of motion [11,12];

$$-\frac{dv}{dt} = \alpha v^2 + \beta v + \gamma \qquad (1)$$

where α, β and γ are the positive constants. αv^2, βv and γ represent the drag force, viscous damping and constant friction, respectively. The analytical solution of this differential equation is available. For $\alpha \neq 0$,

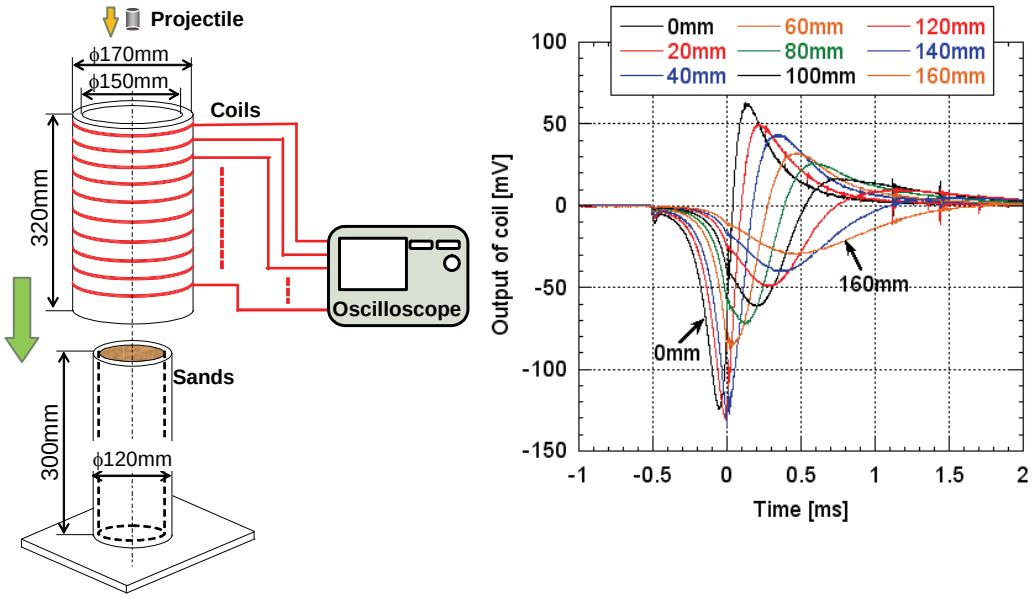

Fig. 7 Penetration velocity measurement system using magnet-coil gage (left) and the examples of the output signals of coil (right)

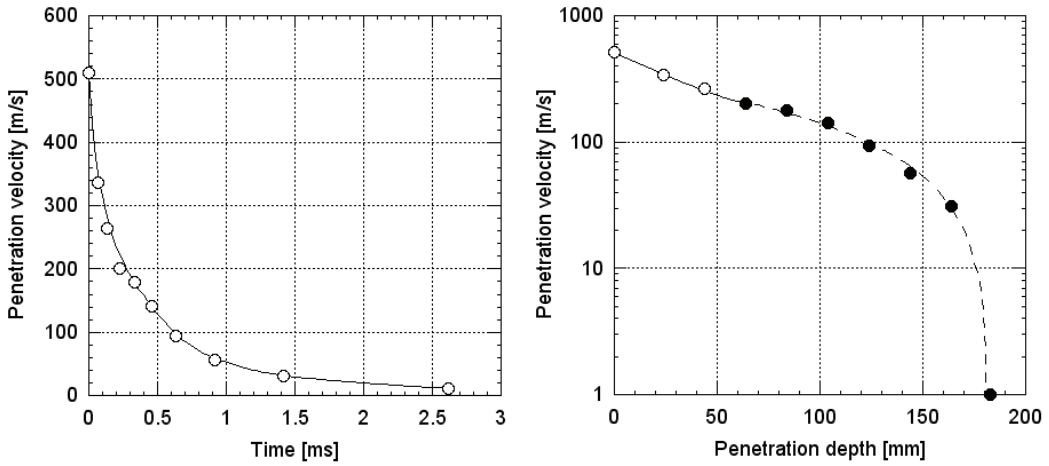

Fig.8 Time history of projectile velocity during penetration (left) and the relation between penetration velocity and penetration depth (right)

$$t=\begin{cases} C-\dfrac{2}{\sqrt{|D|}}\tan^{-1}\dfrac{2\alpha\upsilon+\beta}{\sqrt{|D|}} & (D<0) \\ C+\dfrac{2}{2\alpha\upsilon+\beta} & (D=0) \\ C-\dfrac{1}{\sqrt{D}}\ln\dfrac{2\alpha\upsilon+\beta-\sqrt{D}}{2\alpha\upsilon+\beta+\sqrt{D}} & (D>0) \end{cases} \quad (2)$$

where $D=\beta^2-4\alpha\gamma$. For $\alpha=0$ and $\beta\neq 0$,

$$t=C-\frac{1}{\beta}\ln|\beta\upsilon+\gamma| \quad (3)$$

and for $\alpha=\beta=0$ and $\gamma\neq 0$,

$$\upsilon=-\gamma t+C \quad (4)$$

Moreover, the displacement of the projectile u can be obtained by integrating υ for t. Fig. 9 shows some examples of the solution. Here we set $\upsilon(0)=1$ and $du/d\upsilon|_{t=0}=(1/\upsilon)d\upsilon/dt|_{t=0}=-1$. Compared with Fig.8, it is realized that the initial stage of the penetration is mainly governed by the drag force term, and the latter stage is controlled by the other two terms.

Here we consider the one-dimensional Rankine-Hugoniot equations. The pressure applied to the projectile is

$$P-P_0=\rho_0 Uu \quad (5)$$

where ρ_0 and P_0 is the pressure before impact ($P_0\approx 0$), U is the shock wave speed and u is equal to the projectile speed if we assume that the stiffness of the projectile is sufficiently larger than that of sand deposit. According to the previous experimental data [13-16], the shock wave velocity of most of the materials can be described as follows:

$$U=C+Su \quad (6)$$

where C is the sound speed of the material, and S is the dimensionless material parameter. Accordingly we obtain

$$P=\rho_0(C+Su)u \quad (7)$$

and together with the simple equation of motion (eq(1)),

$$\alpha=\frac{\rho_0}{\rho_P}\frac{S}{L_P},\quad \beta=\frac{\rho_0}{\rho_P}\frac{C}{L_P} \quad (8)$$

where ρ_P and L_P are the density and the length of the projectile, respectively.

In our impact experiment, $\rho_0=1.35(g/cm^3)$, $\rho_P=3.48(g/cm^3)$, $L_p=26(mm)$. The bulk sound speed of the sand deposit under a low confining pressure (1.0 to 3.0 (kPa)) can be

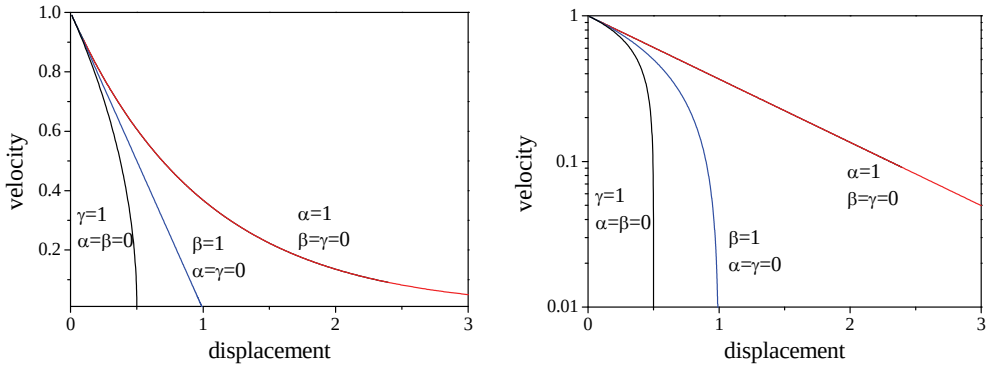

Fig.9 Examples of the solution of Eq.(1). Linear plot (left) and semi-log plot (right).

roughly estimated as 50 to 100 (m/s) [17, 18]. Fig. 10 shows the analytical results using the above physical parameters. Good agreement with experimental observation (Fig. 8) is obtained when $S = 0.75$, which is about half of the typical value in rock materials ($S \approx 1.5$). This reduction may come from the nature of granular materials that contains a lot of voids. The bulk material parameters of granular assembly, C and S are different from those of solids consisting of the grains. For the first-order approximation neglecting the structural details, the difference is a function of void ratio, and in turn, it is largely related to the grain size distribution.

Fig. 11 shows the evidence of grain crushing after the impact experiment. Crushed grains are found not only in front of the projectile but also in its circumferential area. It is also found that the densely compacted crushed grains cone is formed in front of the projectile. This experimental result implies the importance to consider three-dimensional deformation of granular materials. Also, the energy dissipation due to grain crushing and the evolution of grain size distribution are related to the origin of C and S (there is no reason why they are constant throughout the impact process). In the following sections, we explore the grain scale mechanics involving grain crushing.

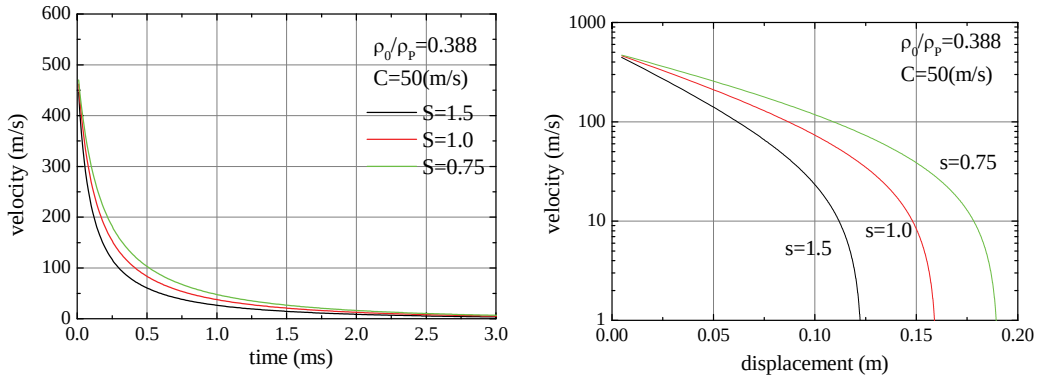

Fig.10 Examples of the solution of Eq.(1) together with Eq.(8). Velocity-time plot (left) and velocity-displacement plot (right).

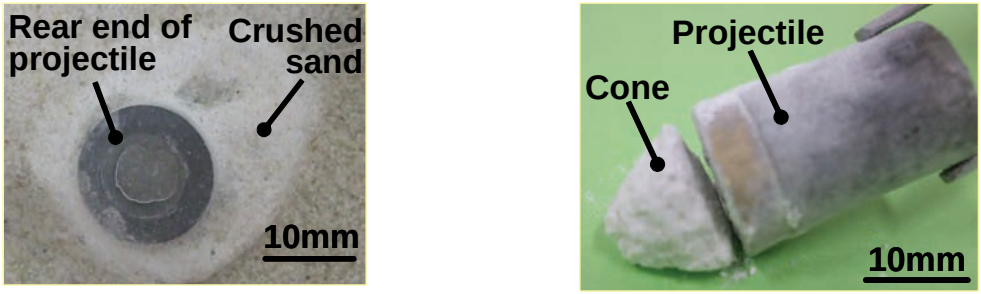

(a) Circumferential crashed sands

(b) Massive crushed sands formed in front of projectile

Fig. 11 Evidence of the grain crushing due to projectile impact

3. **Micro x-ray CT observation on grain crushing and bulk density change in impact experiment:**

In order to investigate the detailed 3-D deformation pattern of a sand deposit due to a projectile impact, we dyed four different colors to Florida coastal sand using printer inks and made horizontal layers. After performing an impact experiment with the same boundary conditions as the one in the previous section, the sand deposit was solidified by resin injection and was cut vertically to observe the deformation of the deposit (Fig. 12). According to the figure, the sand particles located near the projectile penetration path were found to be severely crushed, which can be recognized by changing its color into white; the color of the crushed surface of sand particles. Outside of such crushed region has a rather continuous deformation pattern, and it can be seen that the deformation in the lower layers has a different trend from that in the upper layers. The lower layers exhibit the subduction which follows the projectile penetrating motion (Fig. 13(a)), while the upper layers exhibit upward motion (Fig. 13(b)) possibly due to the expansion accompanied by the lateral shock wave transmission. A clear shear band was observed in both regions which distinguishes the deformed plastic region from outer less-deformed (or elastic) region. Accordingly, we can simply classify the whole field of the sand deposit after impact into three regions; (1) grain crushing region, (2) heavily-deformed (or plastic) region, and (3) lightly-deformed (or elastic) region.

In the grain crushing region, some large voids are observed as shown in Figs 12 and 13. It may be related to the formation of tension cracks caused by (a) the sand compaction due to grain crushing and by (b) the dilation due to the upward deformation in the upper layers. Entrained air during the projectile impact may also affect such void formation. Further investigation is needed for this large void formation behavior.

Next, in order to investigate the grain scale behavior, we picked up a small sample shown in Fig. 13(b) (indicated by a yellow circle) and Fig. 14, to observe its granular structure using a micro focus x-ray CT device (Skyscan 1172). Fig. 14 indicates the location of cross-sections (s530, s330 and s30) shown in Fig. 15. The voxel size of the reconstructed image was 23.175 (micron/voxel). In s530, which is a cross-section closer to the projectile penetration path, severe grain crushing was observed that results in a considerable void

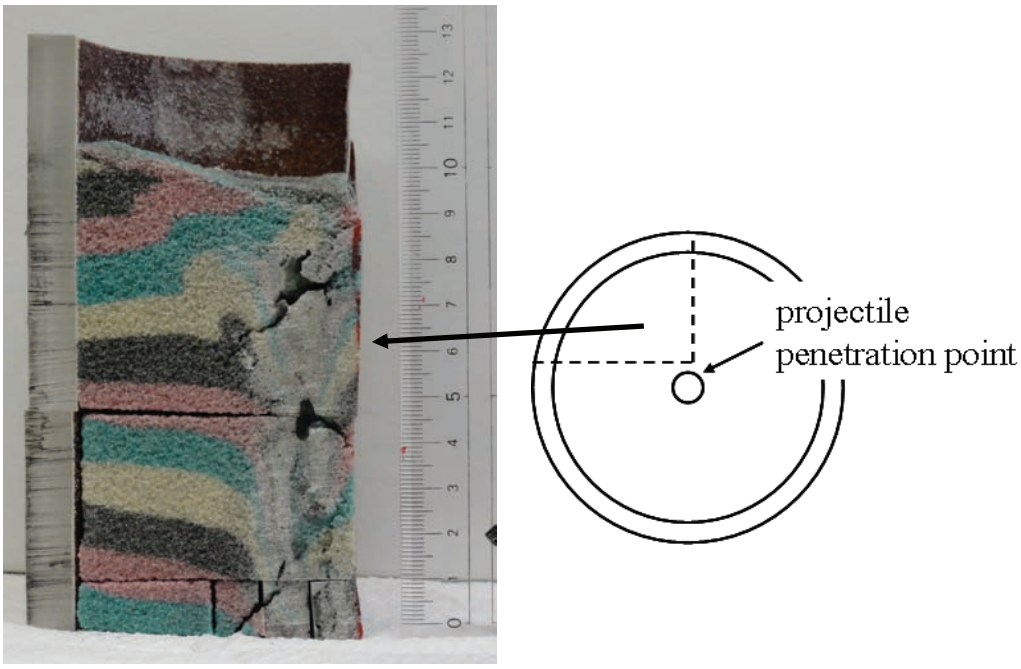

Fig. 12 Vertical cross-section of colored sand deposit after projectile impact

reduction. On the other hand, s30 seems to exhibit little grain crushing though it partly suffers a tension crack. Fig. 16 (top-left) shows the average void ratio with respect to the depth (i.e., different cross-section) of the small sample. In order to smear the local void fluctuation out, we computed the average void ratio of small rectangular solid regions A and B shown in Fig. 16 (top-right). In the figure, the depth of the cross-section equals zero at the sample edge furthest from the penetration path. The void ratio near this edge is around 0.7, which agrees with the initial void ratio of the sand deposit. The void ratio gradually decreases with increasing the depth (getting closer to the penetration path) up to around 0.4 at s530. A sudden drop in the void ratio over s530 may include the effect of cutting process. Also, the result of region B includes the effect of large void (crack). Comparing the deformation pattern observed in Fig. 16 (bottom), it can be said that the average void ratio at grain crushing region is around 0.4 in this experiment, and it gradually increases up to the initial void ratio.

Grain crushing is related to the maximum pressure that the material experienced, but it is difficult to measure it in such an impact experiment. Therefore, in the next section, we perform a series of one-dimensional compression tests in quasi-static loading to explore the relation between the applied pressure, grain crushing, and the resulting void ratio.

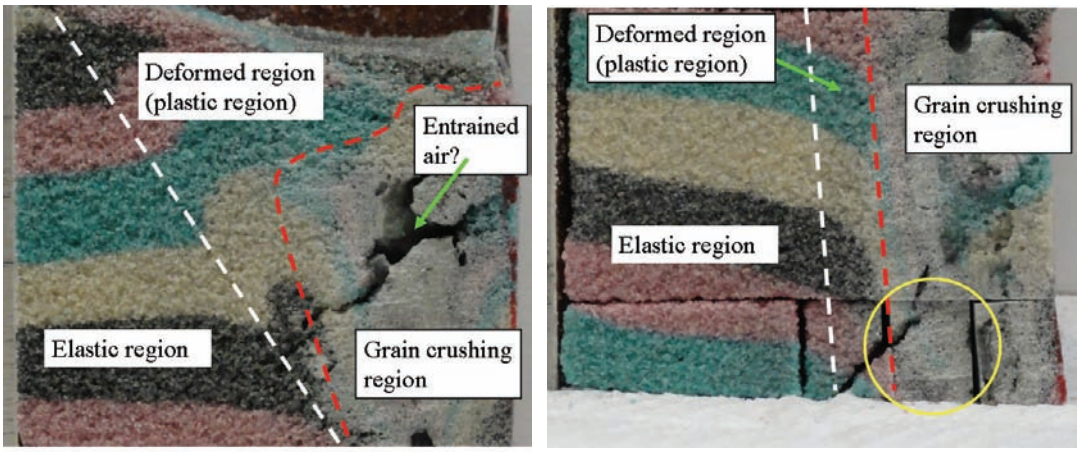

(a) Upper region (b) Lower region

Fig. 13 Three regions ((1) grain crushing region, (2) heavily-deformed (or plastic) region, and (3) un-deformed or lightly-deformed (or elastic) region)

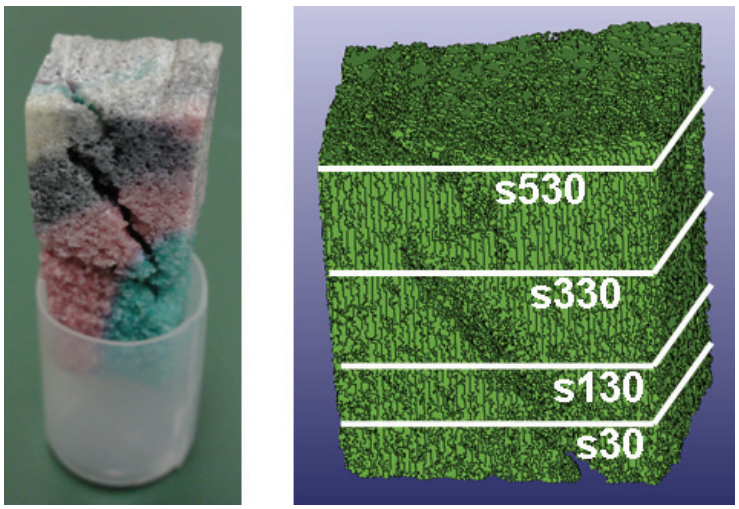

(a) small sample (b) visualized cross-sections

Fig. 14 Small sample picked up from lower grain crushing region

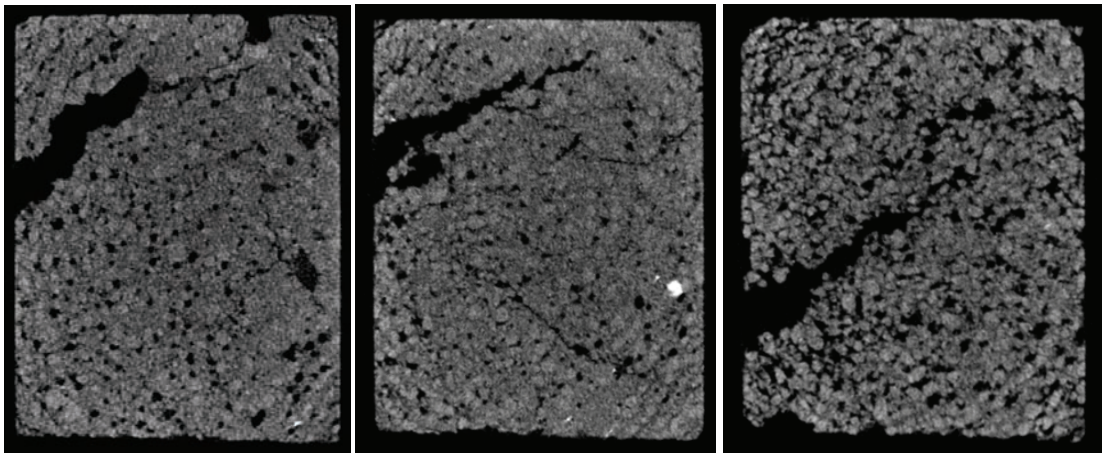

(a) s530 (b) s330 (c) s30

Fig. 15 CT images for three different cross sections. Severer grain crushing is observed in the front section (s530) close to the projectile penetration path. For a single cross section, right-hand side is more severely crushed.

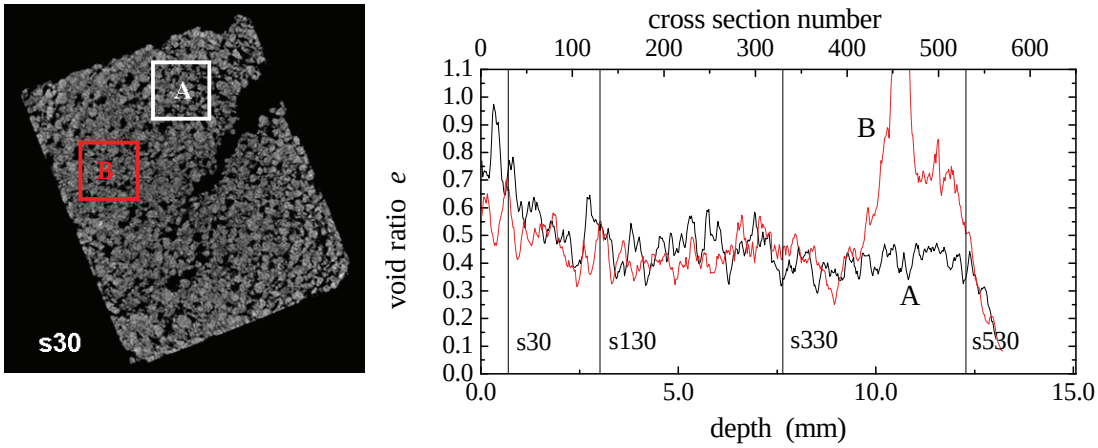

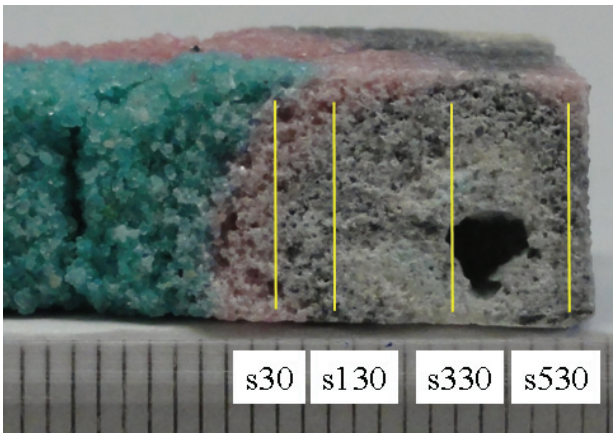

Fig. 16 Small sections A and B where void ratio was measured (top-left), local void ratio distribution obtained from CT images (top-right), and the side view of the specimen corresponding to top-right figure (bottom)

4. One-dimensional compression test under quasi-static loading:

This section describes one-dimensional compression test of Florida coastal sand (the same sand as the one used in the previous sections) under quasi-static loading. Table 1 shows the basic information of the experiment. The sand specimen was prepared in a loose condition (void ratio e=0.93 for case 1) or a medium dense condition (e=0.70 for case 2 and 0.73 for case 3) in a stainless vessel (inner diameter=6.0mm, depth=12.2mm) (Fig. 17). Then one-dimensional compression was applied to the specimen with the displacement-controlled stainless cylinder (whose diameter is almost same as the vessel inner diameter). The applied strain rate is $28*10^{-4}$ (1/s), $29*10^{-4}$(1/s), and $2.0*10^{-4}$ (1/s) for case 1, 2 and 3, respectively. The maximum stress applied was about 0.3(GPa), which is the capacity of the loading frame used in this experiment. Fig. 18 shows the sand particles before and after the experiment (case 1). It is clear that severe grain crushing took place due to high compression. Fig. 19 shows the so-called e-log(p) relation (relation between the void ratio and the compressional

Table 1 Details of 1D compression test

Material: Florida coastal sand		
Mean diameter:		0.37(mm)
Vessel: Stainless steel		
Vessel inner diameter		6.0(mm)
Vessel height		12(mm)
Test case	Initial void ratio	Strain rate $\times 10^{-4}$ (1/s)
1	0.93	29
2	0.70	28
3	0.73	2.0

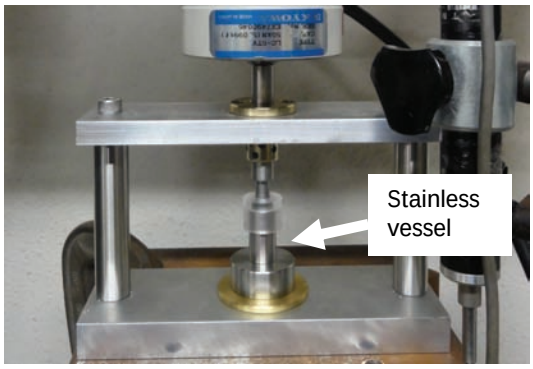

Fig. 17 Setup of the test apparatus

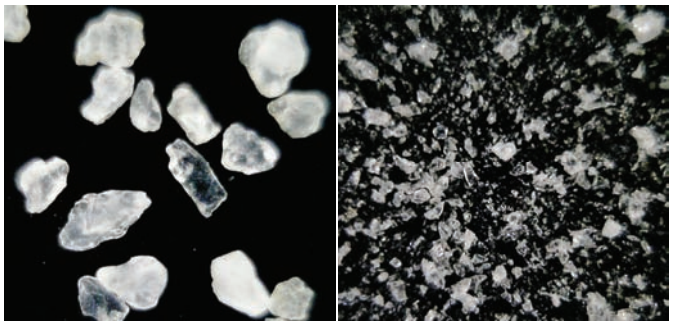

(a) before compression (b) after compression

Fig. 18 sand particles before and after compression

stress in log scale). The solid curves are the experimental results, while the dashed curves are a model response that will be discussed later. The experimental results agree well with the well-known relation consisting of an elastic regime (the curve of relatively smaller inclination at lower pressure) and a plastic consolidation regime after the compressive stress exceeds a threshold yield stress. This yield stress corresponds to the grain crushing stress and it is about 0.02 to 0.04 (GPa) for the sand used in this study. The Pressure larger than this yield stress results in drastic reduction of void ratio. This is because the inter-granular voids are filled with the small fragments generated by grain crushing, which leads to the void ratio reduction. The mechanism of this grain crushing and void ratio reduction is further studied by numerical simulation in the next section.

The effect of the strain rate seems to be negligible in this range. In this quasi-static compression regime, void ratio of 0.4 is attained by the pressure of about 0.1 to 0.2 (GPa).

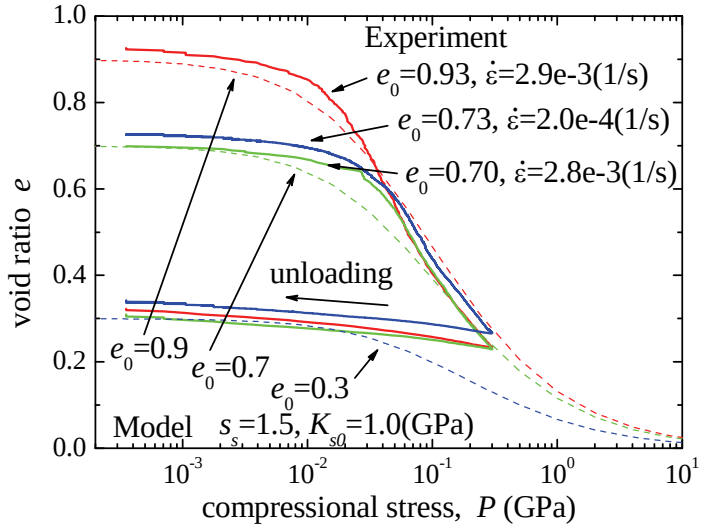

Fig. 19 e-log(p) curve

5. Numerical simulation of grain crushing using DEM (Discrete Element Method):

In order to investigate the grain crushing behavior due to compressive force and the resulting evolution of grain size distribution, a series of one-dimensional compression test are performed using 2-D Discrete Element Method. Crushable grains are modeled with random packing of slightly polydispersed circular elements bonded together (Fig.20(a)). According to the Brazilian test (a single grain crushing test by compressing it with two horizontal plates), the crushing stress $\sigma_f = p_f / D^2$, where p_f is the compression force and D is the grain diameter, decreases with increasing grain size (Fig.20(b)). This tendency is basically in agreement with the real geological grains.

Using such grains, four specimens of different grain size distribution are prepared (B1, B2, B3 and B4 in Figs. 21 and 22). Then gradually increased vertical load, p, is applied

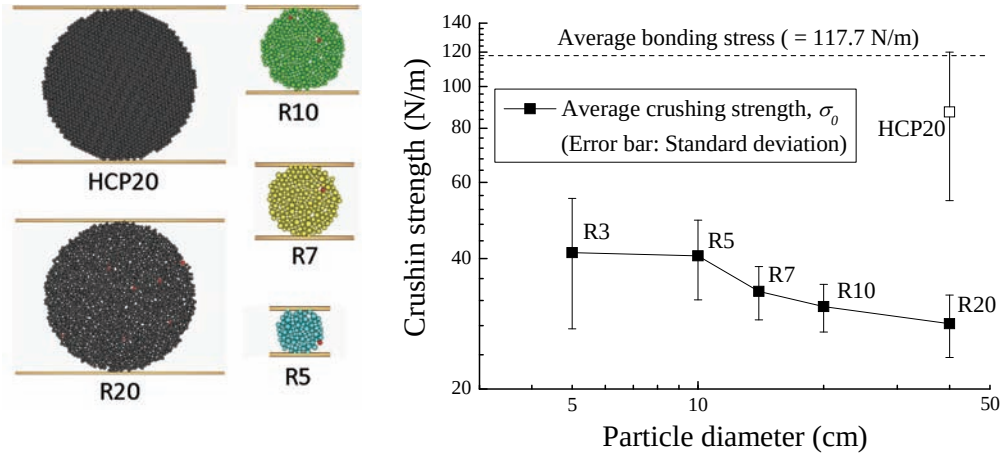

(a) Crushable grain model

(b) Crushing stress with respect to grain diameter

Fig. 20 2-D DEM crushable grain model

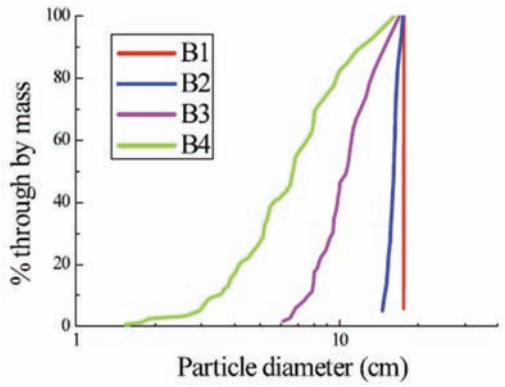

Fig. 21 initial grain size distribution for four specimens (B1 to B4)

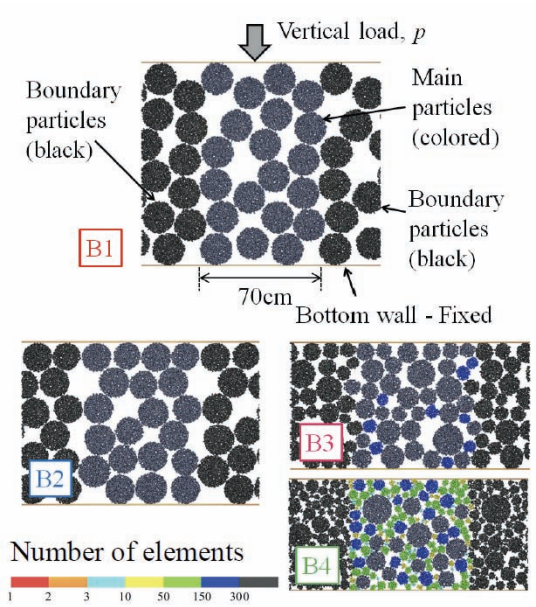

Fig. 22 Initial configuration of four specimens

to the specimens to obtain the relation between p and void ratio e (Fig.23). It is found that the grain crushing occurs at around σ_V =10 to 20 (N/m), which is 1/2 or 1/3 of the single grain crushing stress, primarily because of the force chain structure formed in the granular assembly. Moreover, all the specimens converge into a unique curve after sufficient vertical load application. Fig. 24 shows the initial and the final ($p = 200(kN)$) grain size distributions of all the specimens. The final distributions are almost unique, which is referred to as "critical grading" [19,20]. This critical distribution implies that a certain percentage of the larger grains survive under the very high compressive stress even though their crushing stress is rather smaller than the smaller grains. This is because the larger grains surrounded by smaller grains are subjected to the isotropic internal stress condition from a large number of contact points. Since the grain crushing is caused by the deviatoric stress component, the larger grains survive and eventually critical grading is attained. If such a mechanism works in various scale at the same time, the critical grading must have a fractal nature. Fig. 25 is the cumulative grain size distribution which indicates the distribution has the fractal dimension, D_F of about 1.8. The both edge of the distribution (related to the smallest and the largest grains) is affected by the computational limitation.

Grading change directly leads to the change of the stable void ratio range, which may cause the plastic compression observed in Fig.15. After getting the critical grading, grain crushing hardly occur, and the material behaves not as a granular material any more, but as a continuum solid with little pore. In this phase, usual Hugoniot equation of state can be applied.

Consequently, it is found to be important to consider the three phases; (1) elastic regime as a granular matter, (2) plastic regime due to grain crushing, and (3) Hugoniot solid regime. Based on these phases, more realistic equation of states of granular materials can be modeled.

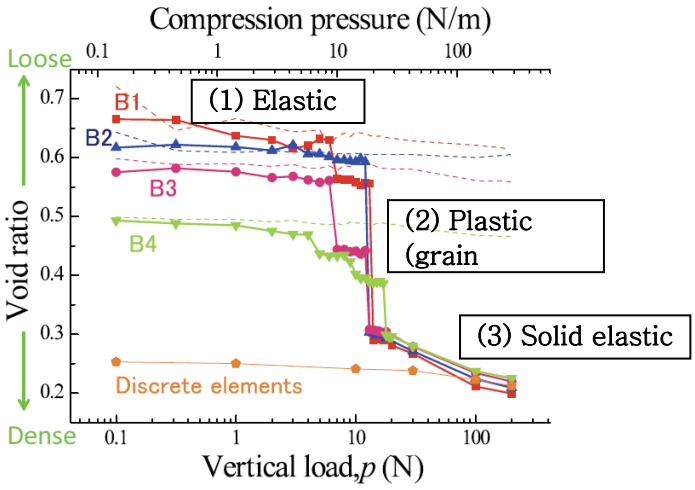

Fig. 23 Void ratio decrease with increasing vertical load

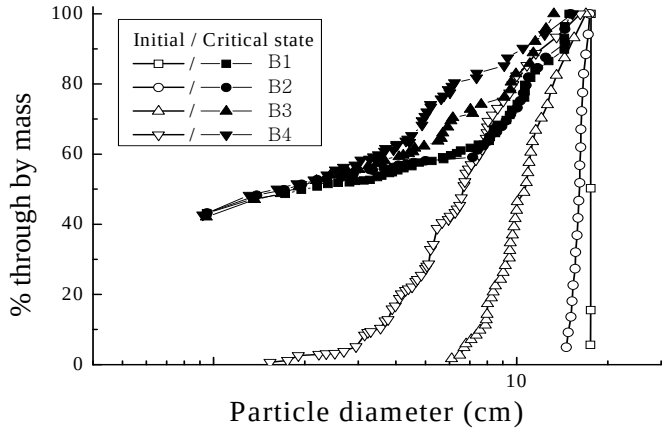

Fig. 24 Evolution of grain size distribution for four specimens

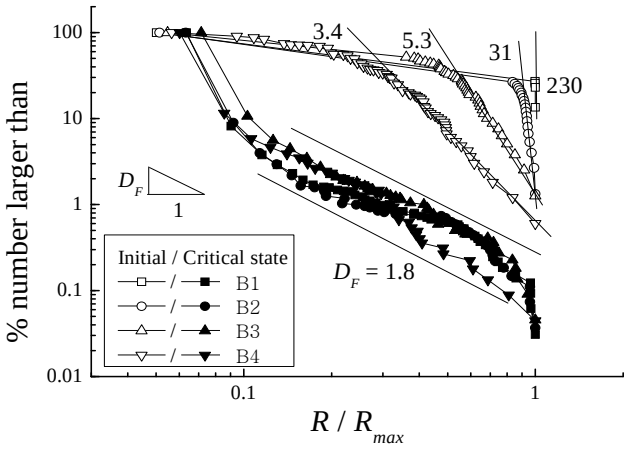

Fig. 25 Fractal grain size distribution

6. Application of Hugoniot equations in granular materials from quasi-static loading to high-speed impact loading:

Here we begin with the basic 1-D Rankine-Hugoniot equations, and then extend to granular materials. Three conservation laws for the mass, the momentum and the energy are described respectively as follow:

$$\rho_0 U = \rho(U-u) \tag{9}$$

$$P - P_0 = \rho(U-u)u = \rho_0 U u \tag{10}$$

$$E - E_0 = \frac{1}{2}(P+P_0)\left(\frac{1}{\rho_0} - \frac{1}{\rho}\right) \tag{11}$$

where U and u are the velocities of the shock wave and the rigid piston with which the shock is applied, ρ, P, E are the density, the pressure and the internal energy per unit weight, respectively, of the compressed medium, and the quantities with the subscript 0 are those of the medium at the initial state (Fig. 26).

Since this 1-D impact problem contains four unknown quantities, ρ, U, P, and E, we need one more equation to close the problem, which is the Equation of State (EOS) of the medium. As described above, a considerable number of impact experiments suggest the following EOS:

$$U = c_0 + su \tag{12}$$

where c_0 is the bulk sound speed and s is a non-dimensional material parameter showing the strain-rate dependent nature of the shock wave velocity.

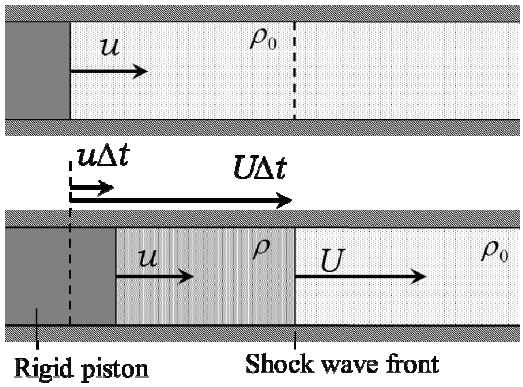

Fig. 26 1D Rankine-Hugoniot impact problem

Since the volumetric strain of the medium, ε_v, can be described by the initial and current densities as:

$$\varepsilon_v = \frac{\Delta V}{V_0} = 1 - \frac{\rho_0}{\rho} \tag{13}$$

we can obtain the following relations:

$$u = \frac{c_0 \varepsilon_v}{1 - s\varepsilon_v} \tag{14}$$

$$U = \frac{c_0}{1 - s\varepsilon_v} \tag{15}$$

$$P - P_0 = \rho_0 \frac{{c_0}^2 \varepsilon_v}{(1 - s\varepsilon_v)^2} = \frac{K_0 \varepsilon_v}{(1 - s\varepsilon_v)^2} \tag{16}$$

where K_0 is the initial volumetric elastic modulus and $c_0 = \sqrt{K_0 / \rho_0}$. One can see clearly that Eq. 16 yields the classical elastic constitutive equation, $P - P_0 = K_0 \varepsilon_v$, when ε_v is sufficiently small, as $(\partial P / \partial \varepsilon_v)_{\varepsilon_v = 0} = K_0$.

Now we consider the EOS of granular materials being composed of solid grains and inter-granular void. Total volumetric strain ε_v and the volumetric strain of solid phase ε_{vs} can be described by the initial and current bulk volumes, V_0 and V, and the initial and current volumes for solid phase, V_{s0} and V_s as follows:

$$\varepsilon_v = \frac{V_0 - V}{V_0} \text{、} \quad \varepsilon_{vs} = \frac{V_{s0} - V_s}{V_{s0}} \tag{17}$$

and the initial and current void ratio are

$$e_0 = \frac{V_0}{V_{s0}} - 1 \text{、} \quad e = \frac{V}{V_s} - 1 \tag{18}$$

Some manipulation give us the following purely geometrical relation:

$$1 - \varepsilon_v = \frac{1 + e}{1 + e_0}(1 - \varepsilon_{vs}) \tag{19}$$

Substituting this equation into Eq. 16, we obtain:

$$P - P_0 = \frac{K_0 \left\{ 1 - (1 - \varepsilon_{vs}) \dfrac{1 + e}{1 + e_0} \right\}}{\left[1 - s \left\{ 1 - (1 - \varepsilon_{vs}) \dfrac{1 + e}{1 + e_0} \right\} \right]^2} \tag{20}$$

Now we consider the limit state (critical state) at very high compression, i.e., $e = 0$:

$$P - P_0 = \frac{K_0 \left(\dfrac{e_0 + \varepsilon_{vs}}{1 + e_0} \right)}{\left[1 - s \left(\dfrac{e_0 + \varepsilon_{vs}}{1 + e_0} \right) \right]^2} \tag{21}$$

The material in this state is regarded as a pure solid (not granular system) which must satisfy the following relation:

$$P - P_0 = \frac{K_{s0} \varepsilon_{vs}}{(1 - s_s \varepsilon_{vs})^2} \tag{22}$$

What we want is the relation between (K_0, s) and (K_{s0}, s_s). First, the critical state at very high compression of those two materials are described respectively as follows:

$P - P_0 \to \infty$ at $\varepsilon_{vs} \to 1 / s_s$

$P - P_0 \to \infty$ at $\varepsilon_{vs} \to (1 + e_0 - e_0 s) / s$

In order to satisfy the condition that the critical ε_{vs} s are identical, we need:

$$s = \frac{s_s (1 + e_0)}{1 + e_0 s_s} \tag{23}$$

Next, we substitute Eq. 23 into Eq. 21 to obtain:

$$P - P_0 = \frac{\left[K_0 \dfrac{(1 + e_0 s_s)^2}{1 + e_0} \left(\dfrac{e_0}{\varepsilon_{vs}} + 1 \right) \right] \varepsilon_{vs}}{(1 - s_s \varepsilon_{vs})^2} \tag{24}$$

and assume that this equation is identical to Eq. 22 in the critical state, $\varepsilon_{vs} \to 1 / s_s$. Then we obtain:

$$K_0 = \frac{(1 + e_0)}{(1 + e_0 s_s)^3} K_{s0} \tag{25}$$

Finally, we can have the EOS of the granular material with the material parameters of solid phase:

$$P - P_0 = \frac{K_{s0}\left(e_0 + \varepsilon_{vs}\right)}{(1 + e_0 s_s)(1 - s_s \varepsilon_{vs})^2} \qquad (26)$$

Fig. 27 shows the comparison between Eqs. 22 and 26. It can be seen that the two relations are almost identical at very high pressure limit both for s=1.0 and for s=2.0, which verifies Eq. 26.

Eqs. 23 and 25 can be used to determine the material parameters of granular materials K_0 and s from those of solid, K_{s0} and s_s, and the initial void ratio, e_0. Fig. 28 shows this relationship for s_s=1.0, 1.5 and 2.0. s for granular materials is smaller than s_s and its reduction rate becomes larger if the initial void ratio e_0 is larger. In any cases, s lies between 1.0 and 2.0, which is in accordance with the existing impact experimental results [13]. For further validation, we used the experimental data for TUFF at Nevada test site [13], which includes the impact experimental data for two types of TUFF rock, which we denote type A and B, respectively, and the data for the uncompressed TUFF powder. Type A TUFF rock has the density ρ_s=1.695(g/cm^3), c_{s0}=1.32(km/s) and s_s=1.41, while type B has ρ_s=1.281(g/cm^3), c_{s0}=0.83(km/s) and s_s=1.39 [13]. Fig. 29 shows the experimental data for TUFF powder together with the model results A ($U = 0.770 + 1.19s$) and B ($U = 0.603 + 1.25s$), which are computed from the type A and B TUFF rock data using Eqs. 23 and 25. The model accuracy is not bad in relatively higher shock wave velocity region. This means that the impact response of a granular material can be predicted by that of the constituent solid. Comparing with the least-square fit [13] the models provide lower shock wave velocity at low particle velocity (i.e., low velocity impact) region, though the experimental data are not sufficient in such a region. We need further investigation on this issue.

Moreover, Fig. 30 shows the relationship between the void ratio and the compressional stress during compression. It can be obtained by assuming that Eq. 22 is satisfied even under compression. Accordingly, ε_{vs} for every $(P - P_0)$ is computed by eq. 22, and then e is computed by eq. 20. The above assumption implies that the total volumetric strain is decomposed into two; the one of solid phase, ε_{vs}, and the one of the void. Fig. 30 shows that the compressional yield stress, which was defined above together with Fig. 19, becomes larger with smaller s_s. The model validation is available in Fig. 19, where K_{s0}=1.0(GPa) and s_s=1.5 provides a good fit for the experimental results.

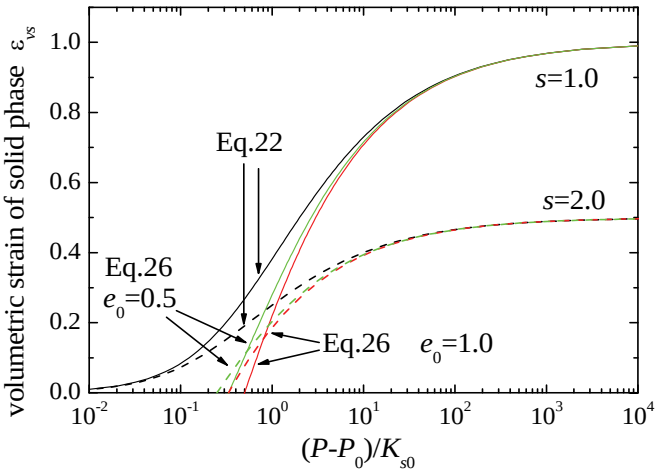

Fig. 27 Comparison between Eq. 22 and Eq. 26

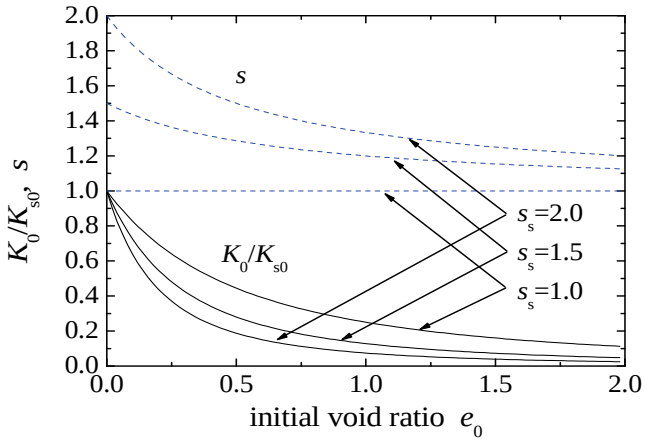

Fig. 28 Compressive elastic modulus and s in terms of initial void ratio

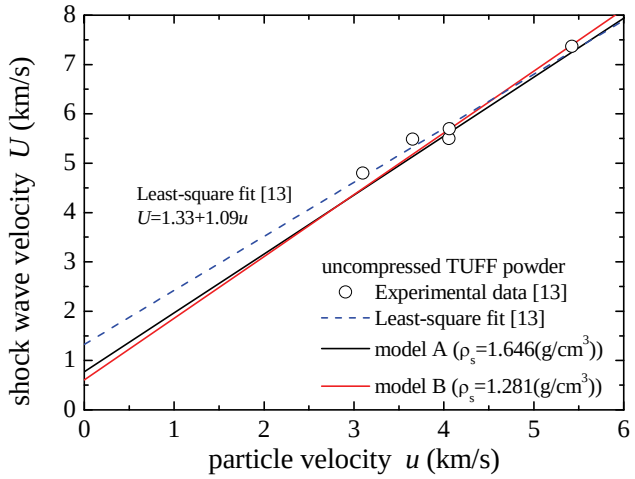

Fig. 29 Impact experimental result for TUFF (solid and powder)

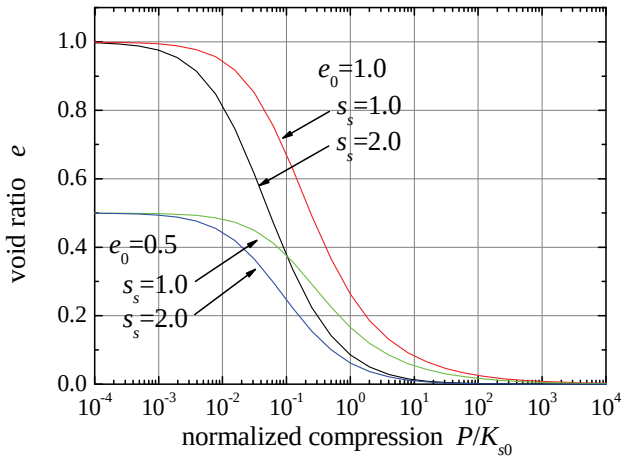

Fig. 30 $e-\log(P/K_{s0})$ relations for different S_s and e_0

7. One dimensional model of projectile penetration into sand deposit:

In this section we demonstrate an application of the EOS described in section 6 into a boundary value problem, the impact experiment into sand deposit shown in section 2. In order to explore the basic response of the proposed EOS and the effect of material parameters on the simulation result with a simple setup, we adopt a one dimensional model as shown in Fig. 31. A sand deposit is discretized horizontally and is assumed to move only in the vertical direction, denoted by x coordination. The equation of motion of sand element i is described as follows:

$$\rho_i l_i A \frac{d^2 x_i}{dt^2} = (P_i - P_{i+1})A - F_i A_H \qquad (27)$$

where ρ_i and l_i are the density and the width of the sand element i, respectively, A is the impact area the projectile of cylinder, $A = \pi D^2 / 4$ (D is the diameter) and A_H is the side area of the sand element, $A_H = \pi D l_i$. In addition, ρ_0 and l_0 correspond to the density and the length of the projectile, i.e., $\rho_0 = \rho_P$ and $l_0 = l_P$.

The compressional stress P and the frictional stress F for each sand element (see Fig. 31) are computed from the following relations:

$$P = \rho_{s0} \frac{{c_{s0}}^2 (e_0 + \varepsilon_{vs})}{(1 + e_0 s_s)(1 - s\varepsilon_v)^2} \qquad (28)$$

$$P = \frac{K_{s0}\varepsilon_{vs}}{(1 - s_s \varepsilon_{vs})^2} \qquad (29)$$

$$F = \mu k_H P \qquad (30)$$

Eqs. 20 and 21 are the same as eqs. 26 and 22, respectively, and eq. 30 is the frictional law with the material parameters k_H, μ which describe the horizontal earth pressure coefficient and internal friction coefficient, respectively, used in classical soil mechanics.

Parameters used in the following simulation are summarized in Table 2. Most of the parameters are directly obtained from the experiment in section 2. $k_H = 0.5$ is a typical value often used in soil mechanics application. Since there is little information on μ for high velocity friction in granular materials, we perform a parametric study.

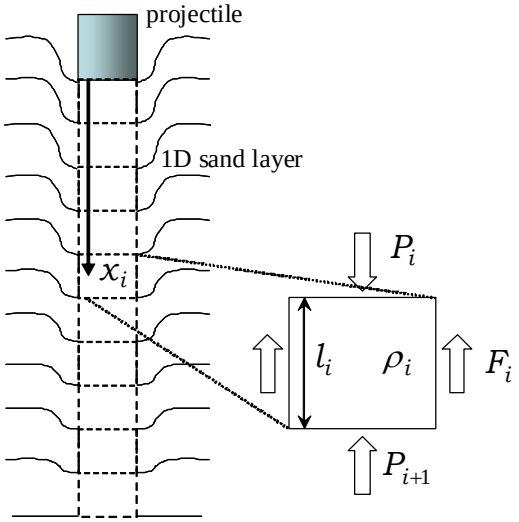

Fig. 31 Setup of one-dimensional simulation

Table 2 Parameters used in the simulation

sand layer	
initial void ratio e_0	1.0 (loose) 0.7 (medium dense)
thickness of sand layer H	100 (cm)
particle density ρ_s	2.7 (g/cm^3)
compressive modulus K_{s0}	1.0 (GPa)
horizontal earth pressure coefficient K_H	0.5
parameter s_s	1.5
side friction μ	0, 0.005, 0.01
projectile	
density ρ_P	3.48 (g/cm^3)
length l_P	2.6 (cm)
diameter D	1.5 (cm)
initial impact velocity u_p	100, 200, 500 (m/s)
computational parameter	
mesh size l	$H/200$ (cm)
time increment Δt	1.0×10^{-9} (s)

Fig. 32 plots the time history of projectile position. It is obvious that the final penetration depth increases with decreasing side friction μ. This side friction of granular solid is usually 0.5 to 1.0 in quasi-static deformation. When we assign such value, the final penetration depth becomes much smaller than the experimental result in section 2. This implies that the dynamic friction due to high-speed projectile penetration is much smaller than that in quasi-static shear.

Fig. 33 shows the relation between the projectile velocity and vertical position. The basic trend is in good agreement with the experimental result shown in Fig. 8 (right). According to Allen et al. [11], the slope of $v_P - x_P$ curve changes when the projectile velocity exceeds the sound speed of the medium, which is $c_0 = \sqrt{K_0/\rho_0}$ =308(m/s) by eq. 25. In Fig. 33, the slope of $v_P - x_P$ curve seems to be changed at around v_p =200(m/s). In order to examine this slope change behavior in details, Fig. 34 plots the $v_P - x_P$ curves for various initial projectile velocities, u_p. When u_p =100(m/s) < c_0, the slope change

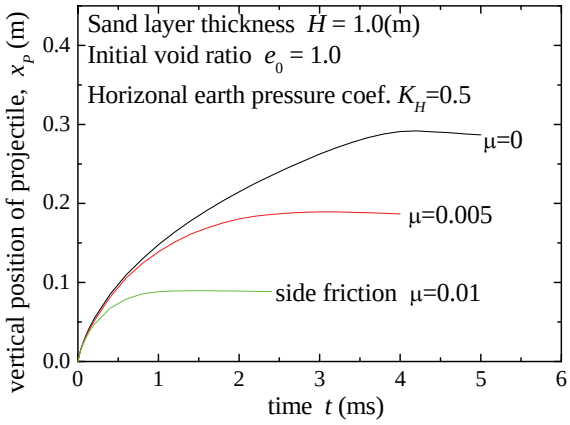

Fig. 32 time history of vertical position of projectile

cannot be observed. This implies the existence of critical velocity governing the slope change, but this critical velocity does not perfectly correspond to the sound speed.

Fig. 35 indicates the evolution of void ratio at different depth of the sand deposit during projectile penetration. Being affected by the EOS adopted in the simulation, the shock wave velocity transmission and the resulting void ratio distribution is much more complicated than those assumed in the 1D Hugoniot equations, though each material element behaves as the assigned EOS (Fig. 36). This implies that the projectile behavior is also affected by such complicated behavior of the sand deposit.

Note that the assigned EOS is rate independent, and still the projectile behavior is rate dependent because of the sand deposit behavior described above.

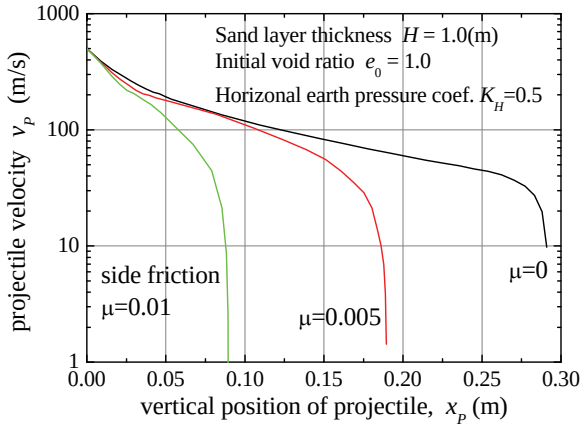

Fig. 33 projectile velocity vs. vertical position of projectile (1): effect of internal friction

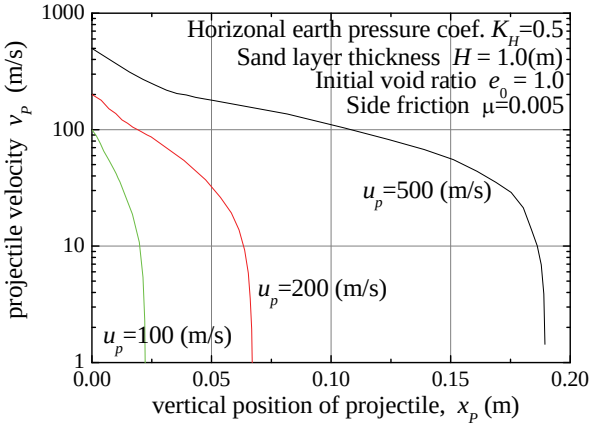

Fig.34 projectile velocity vs. vertical position of projectile (2): effect of the initial velocity of projectile

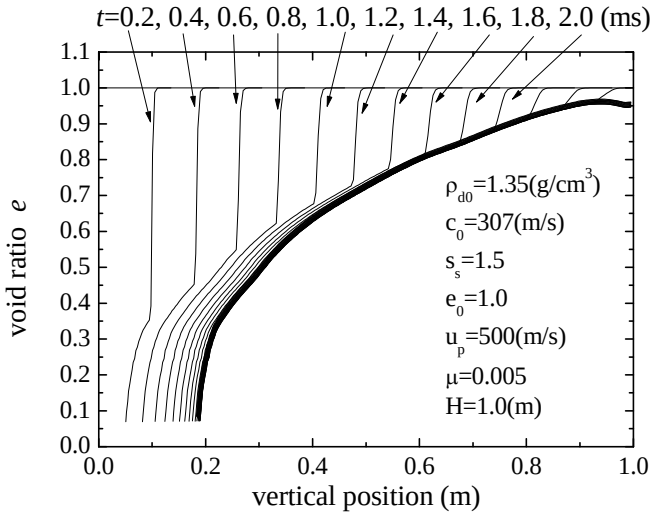

Fig. 35 Evolution of void ratio at different depth of the sand deposit

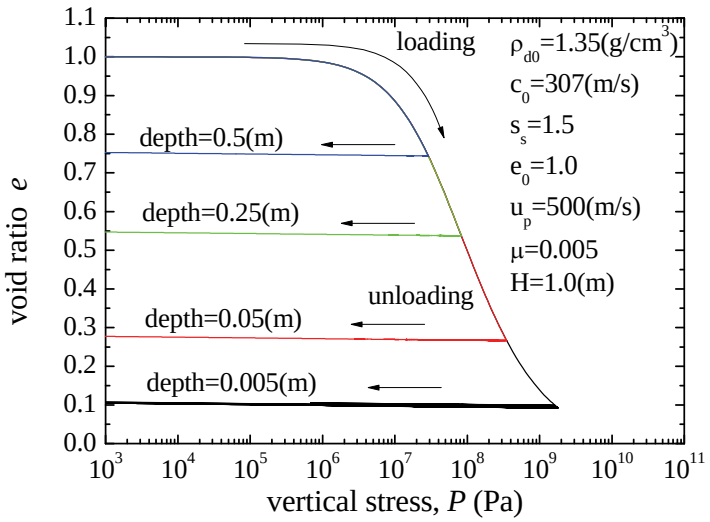

Fig.36 Constitutive response of the granular material at different initial depth

8. Conclusions:

We aimed at clarifying the high-speed impact behavior of granular materials such as sand deposit in this research. Since the granular materials subjected to very high pressure suffer considerable grain crushing, we tried to model it in a phenomenological way. What we intended is to construct the EOS which covers wide range of deformation rate; from quasi-static deformation to high-speed impact, because the projectile deceleration process is affected not only by the initial high-speed regime but also the subsequent slow deformation regime. A very useful finding for this purpose is that the widely used relation between the shock wave velocity U and the projectile impact velocity u; $U = c_0 + su$ can be connected mathematically with the classical soil mechanics relation between the void ratio e and the applied pressure p. Therefore, the obtained expression can be validated both with impact experiment and with quasi-static 1D compression test. Moreover, we also found that the material parameters c_0 and s for granular materials can be obtained from those

for the host rock. In the last section, we demonstrated the applicability of the proposed EOS into high-speed projectile impact experiment. It turned out that the projectile deceleration behavior observed in the experiment is a consequence of the complicated compression behavior of sand deposit.

It is worth mentioning that the proposed EOS can be combined with the friction model, which results in a popular soil mechanics model called Cam-clay model [21]. The application of this model enables us to perform more realistic simulation of projectile impact experiment. At the same time, the grain scale simulation by DEM is also important to clarify the physical origin of the proposed EOS.

REFERENCES:

[1] de Pater, I, Lissauer, J.J: Planetary sciences, second edition, Cambridge university press, 2010.
[2] Melosh, H.J.: Impact cratering –a geologic process-, Oxford university press, 1989.
[3] Akira Sawaoka: Shock waves in materials science, Springer-Verlag, 1993.
[4] Hetherington, J.G., Smith, P.D.: Blast and Ballistic Loading of Structures, Butterworth -Heinemann Ltd, 1994.
[5] Duran, J.: Sands, Powders, and Grains: An introduction to the physics of granular materials, Springer-Verlag, 2000.
[6] Hermann, H.J: Granular Matter, Physica A, 313, 188-210, 2002.
[7] Xue, K., Bai, C.H.: Spherical shock-wave propagation in three-dimensional granular packings, PHYSICAL REVIEW E 83, 021305, 2011.
[8] Dressler, B.O., Reimold, W.U.: Terrestrial impact melt rocks and glasses, Earth-Science Reviews, 56, 1-4, 250-284, 2001.
[9] Maxwell, D.E., Simple Z model of cratering, ejection and the overturned flap, Impact and explosion cratering, Roddy, D.J., Pepin, R.O. and Merrill, R.B. (eds.), Pergamon press, 1003-1008, 1977.
[10] Workshop on Particulate Materials in Extreme Environments, Coordinator: Cooper, W.L., Lawrence Livermore National Laboratory, 2010.
(http://mpdc.mae.cornell.edu/Publications/PDFiles/INVITEDTALKS/PMEE2010Announcement .pdf)
[11] W.A. Allen, E.B. Mayfield and H.L. Morrison, Dynamics of Projectile Penetrating Sand, J. Appl. Phys., Vol.28, pp.370-376, 1957.
[12] M.W. Backman and W. Goldsmith, The Mechanics of Penetration of Projectiles into Targets, J. Engng. Sci., Vol.16, pp.1-99, 1978.
[13] Marsh, S.P. (Ed.): LASL shock Hugoniot data, University of California press, Berkeley, 1980.
[14] van Thiel, M.: Compendium of shock wave data, UCRL-50108, Lawrence Livermore Laboratory, Livermore, 1977.
[15] Kohn, B.J.: Compilation of Hugoniot equations of state, AFWL-TR-69-38, Air Force Weapons Laboratory, new Mexico, 1969.
[16] Trunin, R.F.: Shock compression of condensed materials, Cambridge University Press, Cambridge, 1998.
[17] Hardin, B.O., Richart, F.E.: Elastic wave velocities in granular soils, Proc. ASCE, 89 SM1, 33-65, 1963.
[18] Matsushima, T., Micromechanics-based constitutive models (4.3) , in Elasto-plastic constitutive models of soils, Tobita et al. eds., Japanese Geotechnical Society, 2009 (in Japanese).
[19] McDowell, G.R., Bolton, M.D. and Robertson, D. “The fractal crushing of granular materials” Journal of Mechanical Physics Solids, 44(12), 1996, pp 2079-2102.
[20] Wood, D.M., Maeda, K., “Changing grading of soil: effect on critical states”, Acta Geotechnica, 3, 2008, pp 3-14.

[21] Schofield, A., Wroth, P.: Critical state soil mechanics, McGraw-Hill, 310p, 1968.

List of Publications:

Ueda, T., Matsushima, T., Yamada, Y: Effect of particle size ratio and volume fraction on shear strength of binary granular mixture, Granular Matter (2011) 13:731–742

Ueda, T., Matsushima, T., Yamada, Y.: Effect of grade changing due to grain crushing on the compressibility of granular materials, Proc. ICAGE (International Conference on Advances in Geotechnical Engineering, 165-170, 2011.

Ueda, T., Matsushima, T., Yamada, Y.: Micro structures of granular materials with various grain size distributions, Powder Technology, Vol.217, February 2012, pp.533-539.

Ueda, T., Matsushima, T., Yamada, Y: Ball-bearing effect on shear behavior of binary granular mixture, Journal of Geotechnical Engineering JSCE A2, 68(1), pp.1-9, 2012.

Ueda, T., Matsushima, T., Yamada, Y: DEM simulation on the one-dimensional compression behavior of various shaped crushable granular materials, Granular Matter, accepted.

Matsushima, T., Watanabe, K.: High speed projectile impact to sand deposit: Soil mechanics interpretation of Hugoniot equation of state, submitted.